THE ASTROPHYSICAL JOURNAL, 511:149–156, 1999 January 20

MEASUREMENT OF THE MULTI-TeV GAMMA-RAY FLARE SPECTRA OF MARKARIAN 421 AND MARKARIAN 501

F. KRENNRICH,[1] S. D. BILLER,[2] I. H. BOND,[3] P. J. BOYLE,[4] S. M. BRADBURY,[3] A. C. BRESLIN,[4] J. H. BUCKLEY,[5] A. M. BURDETT,[3] J. BUSSONS GORDO,[4] D. A. CARTER-LEWIS,[1] M. CATANESE,[1] M. F. CAWLEY,[6] D. J. FEGAN,[4] J. P. FINLEY,[7] J. A. GAIDOS,[7] T. HALL,[7] A. M. HILLAS,[3] R. C. LAMB,[8] R. W. LESSARD,[7] C. MASTERSON,[4] J. E. MCENERY,[9] G. MOHANTY,[1,10] P. MORIARTY,[11] J. QUINN,[12] A. J. RODGERS,[3] H. J. ROSE,[3] F. W. SAMUELSON,[1] G. H. SEMBROSKI,[6] R. SRINIVASAN,[6] V. V. VASSILIEV,[12] AND T. C. WEEKES[12]

Received 1998 July 22; accepted 1998 August 27

ABSTRACT

The energy spectrum of Markarian 421 in flaring states has been measured from 0.3 to 10 TeV using both small and large zenith angle observations with the Whipple Observatory 10 m imaging telescope. The large zenith angle technique is useful for extending spectra to high energies, and the extraction of spectra with this technique is discussed. The resulting spectrum of Markarian 421 is fitted reasonably well by a simple power law: $J(E) = E^{-2.54\pm0.03\pm0.10}$ photons m^{-1} s^{-1} TeV^{-1}, where the first set of errors is statistical and the second set is systematic. This is in contrast to our recently reported spectrum of Markarian 501, which over a similar energy range has substantial curvature. The differences in TeV energy spectra of gamma-ray blazars reflect both the physics of the gamma-ray production mechanism and possibly differential absorption effects at the source or in the intergalactic medium. Since Markarian 421 and Markarian 501 have almost the same redshift (0.031 and 0.033, respectively), the difference in their energy spectra must be intrinsic to the sources and not due to intergalactic absorption, assuming the intergalactic infrared background is uniform.

Subject headings: BL Lacertae objects: individual (Markarian 421, Markarian 501) — galaxies: active — gamma rays: observations

1. INTRODUCTION

Three blazars, Markarian 421 (Punch et al. 1992), Markarian 501 (Quinn et al. 1996), and 1ES 2344+514 (Catanese et al. 1998), have been detected at TeV energies. At GeV energies, the EGRET instrument aboard the Compton Gamma Ray Observatory found only upper limits for Markarian 501 (Catanese et al. 1997) and 1ES 2344+514 (D. J. Thompson 1996, private communication). Markarian 421 was detected by EGRET, but only very weakly (Thompson et al. 1995). While blazar emission for X-ray–selected objects at lower energies (up to about 1–100 keV) is almost certainly due to synchrotron emission from a beam of highly relativistic electrons, the GeV/TeV emission forms a second component usually attributed to inverse Compton scattering of relatively low-energy photons by the electron beam (see, e.g., Sikora, Begelman, & Rees 1994) or perhaps to pion photoproduction by a proton component of the beam (see, e.g., Mannheim 1993). The inverse Compton models predict typical blazar gamma-ray energy cutoffs from 10 GeV to about 30 TeV, whereas proton beam models allow gamma-ray energies exceeding 100 TeV. Spectrum measurements at both the low-energy end (perhaps probing the energy threshold of the second component) and the high-energy end (perhaps showing an energy cutoff) are important for constraining models.

The TeV gamma-ray spectra of extragalactic objects can be modified by differential absorption due to photon-photon collisions with intergalactic IR radiation (Gould & Schrèder 1967; Stecker, De Jager, & Salamon 1992). Indeed, TeV observations of Markarian 421 and Markarian 501 (Zweerink et al. 1997; Krennrich et al. 1997; Aharonian et al. 1997) have been used to set upper limits on the density of intergalactic IR radiation (Stanev & Franceschini 1998; Biller et al. 1998). These upper limits provide the best constraints on infrared densities in the 0.02–0.2 eV regime and do not suffer from local galactic background contributions as are present in direct measurements. At this time no unambiguous evidence has been found for an IR absorption spectral cutoff. In order to infer the magnitude of intergalactic IR background radiation from absorption effects on TeV spectra, it is necessary to have a good model for intrinsic spectra or to have spectra from several objects and assume that the intrinsic TeV spectra of the objects are identical (or at least very similar), or to have detections from many sources and assume that they are similar in a statistical sense. For the redshift range ($z = 0.031$–0.044) of the detected TeV blazars Markarian 421, Markarian 501, and 1ES 2344+514, a recognizable cutoff (optical depth $\sim$1–5) is expected to occur between 5 and 20 TeV (Stecker & De Jager 1997; Stecker et al. 1998).

We have recently published a brief report giving a detailed spectrum of Markarian 501 spanning the energy

[1] Department of Physics and Astronomy, Iowa State University, Ames, IA 50011-3160.
[2] Department of Physics, Oxford University, Oxford, England, UK.
[3] Department of Physics, University of Leeds, Leeds, LS2 9JT, England, UK.
[4] Experimental Physics Department, University College, Belfield, Dublin 4, Ireland.
[5] Department of Physics, Washington University, St. Louis, MO 63130.
[6] Physics Department, National University of Ireland, Maynooth, Ireland.
[7] Department of Physics, Purdue University, West Lafayette, IN 47907.
[8] Space Radiation Laboratory, California Institute of Technology, Pasadena, CA 91125.
[9] Present address: Department of Physics, University of Utah, Salt Lake City, UT 84112.
[10] Present address: LPNHE Ecole Polytechnique, 91128 Palaiseau CEDEX, France.
[11] School of Science, Galway-Mayo Institute of Technology, Galway, Ireland.
[12] Fred Lawrence Whipple Observatory, Harvard-Smithsonian CfA, P.O. Box 97, Amado, AZ 85645-0097.

range 260 GeV–10 TeV derived from observations with the Whipple Observatory gamma-ray imaging Cerenkov telescope (Samuelson et al. 1998). This spectrum was derived from observations made during "high" states of the active galactic nucleus (AGN) that give good statistical precision. Markarian 501 (Quinn et al. 1998) is variable in the TeV energy range showing changes on a timescale of several hours. The data were taken at both standard small zenith angles (SZA) of less than 25° and at large zenith angles (LZA) in the range of 55°–60°. The SZA observations are sensitive to relatively low energies ($E < 5$ TeV), and the LZA observations yield better statistics at high energies. The details of the analysis were not explained in the brief report but are given here. In particular, the characteristics of Cerenkov imaging telescopes relevant for spectral determination change substantially from SZA to LZA observations. In addition, uncertainties in the spectrum, e.g., due to corresponding uncertainties in atmospheric absorption, are also given here. Finally, we have used the flux from the Crab Nebula (which often serves as a standard candle in TeV gamma-ray astronomy) to check spectra extracted from LZA observations against our standard spectrum (Hillas et al. 1999a).

These recent results from Markarian 501 indicate a spectrum that is not consistent with a simple power law in which the flux, J, is proportional to $E^{-\gamma}$, but is more accurately described by a three-parameter curve (parabolic in a plot of log J vs. log E given by $J \sim E - 2.22 \pm 0.04 \pm 0.05 - (0.47 \pm 0.07) \log_{10} E$, where the first set of errors is statistical and the second systematic and E is in TeV. (Previously published spectra of Markarian 501 covered a smaller energy span and were consistent with a simple power law; see, e.g., Bradbury et al. 1997; Aharonian et al. 1997.) In principle, the curvature of the spectrum could arise either from the physics of gamma-ray emission from AGN, from intrinsic absorption, or from absorption in the intergalactic medium.

In addition to Markarian 501, the Whipple Observatory Gamma-Ray Collaboration has a database of both SZA and LZA data for Markarian 421. Fortuitously, these objects have almost identical redshifts: 0.031 for Markarian 421, and 0.033 for Markarian 501. Hence any differences in their TeV spectra must be intrinsic to the AGN and not due to intergalactic absorption, assuming the intergalactic IR background radiation is uniform. Like Markarian 501, Markarian 421 is also highly variable, with changes observed on a timescale as short as 15 minutes (Gaidos et al. 1996). We have previously published a TeV spectrum for Markarian 421 based on a single SZA observation but with very high flux detection lasting only 2 hr (Zweerink et al. 1997). The published spectrum was consistent with a simple power law; i.e., no curvature was required for an acceptable fit. However, the spectrum did not cover as large an energy range as that for Markarian 501, nor did the Markarian 421 spectrum have comparable statistical precision at the high-energy end of the spectrum. Hence it was not possible to draw firm conclusions from a comparison of the two spectra.

Here we present a new TeV spectrum of Markarian 421 based upon both SZA and LZA data taken while the AGN was in a high state of emission. The SZA data set used consists of two flaring detections. The first is the same 2 hr detection (average flux of 7.4 crab units) used to obtain the previously published spectrum (Zweerink et al. 1997), but we have taken additional care in the treatment of energy threshold effects in order to obtain flux values at lower energies. The second detection (27 minutes on source) had an average flux of 2.8 crab units and exhibited a remarkably short rise and fall time of 15 minutes. It occurred 8 days after the first detection. The LZA observations consisted of 1.5 hr (1995 June) of on-source data at zenith angles of 55°–60° with an average flux of 3.3 crab units. The new spectrum is consistent with our previously published result but spans a larger energy range (comparable to that published for Markarian 501) and has better statistics at high energies. The spectrum appears less curved than the Markarian 501 spectrum. We show that the spectra for the two equidistant AGN (Markarian 421 and Markarian 501) clearly differ, and this reflects intrinsic spectral differences near the sites of gamma-ray production. Combined with data for the two AGN at X-ray energies, these spectra constrain models of physical processes in the jets (see Hillas et al. 1999b). The differences also point toward a major difficulty in inferring intergalactic background radiation intensities via TeV photon attenuation.

2. OBSERVATIONS

The observations presented here were made with the Whipple Observatory 10 m imaging Cerenkov telescope. The camera consisted of 109 (until 1996 December 4) or 151 (after 1996 December 4) photomultiplier tubes placed on a 1/4° hexagonal matrix. These cameras covered fields of view of about 2°.7 and 3°.2, respectively. Pulses from each of the photomultiplier tubes were amplified and sent to gated integrating analog-to-digital converters, and, in addition, those from the inner 91 tubes were sent to discriminators with levels corresponding to about 49 photoelectrons. When two of the discriminators fired, a trigger was generated and current pulses from all photomultiplier tubes were integrated for 25 ns and digitized (Cawley et al. 1990). The data were normally taken in an on-off mode in which the source is tracked for typically 28 minutes, and then the same range of elevation and azimuth angles is tracked for another 28 minutes, which gives a background comparison region. The Crab Nebula serves as a standard candle for TeV gamma-ray astronomy, and it was observed using the same camera configurations and ranges of zenith angles that were used for the blazar observations.

As described previously in Samuelson et al. (1998), the Markarian 501 observations were made in the time interval from 1997 February 14 to 1997 June 8 during a high state of the source in 1997 (Protheroe et al. 1998). During this period the camera had 151 pixels, which gave the larger (3°.2) field of view. A total of 16 hr of SZA on-source data were taken at 8°–25°, and 5.1 hr of LZA on-source data were taken at 55°–60°. These observations showed that the flux for the 1997 observing season varied from about 0.2 to 4 times the flux from the Crab Nebula, with an average value of 1.4 (see Quinn et al. 1998). This is a factor of 7 larger than the average flux from the 1996 observing season, which is the basis for identifying it as flare data. We are somewhat arbitrarily defining flare data as that which has a flux level substantially above the average flux as measured for a given source in our observations.

The SZA data for Markarian 421 consists of two detections on 1996 May 7 and 1996 May 15, measured with the 109 photomultiplier tube camera. The first of these was during the highest flux TeV flare observed. It consisted of a

2 hr observation in which the data rate increased steadily, giving a count rate at the end of the run of about 15 gammas minute^{-1} at $E > 350$ GeV, which is 10 times the rate from the Crab Nebula. The average rate during the runs was 7.4 Crab units. During the flare the AGN was observed continuously, and hence background comparison regions were taken from the same range of elevation and azimuth angles but from other nights; however, because of the strength of the signal, the data are almost free of background after selection of gamma-ray–like images. The results are insensitive to the exact background runs used (Zweerink et al. 1997; Zweerink 1997). The second detection 8 days later consisted of 27 minutes of on-source observations with corresponding off-source data. The average flux was 2.8 crab units, and the data show a remarkable peak with a rise and fall time of only 15 minutes. The Crab Nebula database was measured with the same camera during the 1995–1996 season and consists of 49 on/off pairs giving the Crab Nebula spectrum reported by Hillas et al. (1999a).

Observations of Markarian 421 at LZA were carried out in 1995 with the 109 pixel camera (Krennrich et al. 1995), and the detection of 5–8 TeV gamma rays was reported earlier (Krennrich et al. 1997). For the spectral analysis presented here, we used a subset of the data for which the range of zenith angles is 55°–60°, where we have adequate observations of the Crab Nebula to obtain a spectrum. This allows us to use the Crab Nebula to test the LZA analysis procedure and show that it is consistent with spectra derived at SZA. In addition, we required that Markarian 421 was in a flare state, which gave a total of three on-off pairs of data measured on 1995 June 20, 29, and 30, with an average flux from the AGN of 3.3 crab units, comparable to that of the 1996 May 15 flare (an average of 2.8 crab units).

Data from observations of the Crab Nebula at zenith angles between 55° and 60° were collected during 1995, 1996, and 1997 using both the 109 and 151 pixel cameras. A total of 17 on-off pairs (8 hr on source) were used for the derivation of the energy spectrum of the Crab Nebula. The spectra derived from the two cameras were in agreement.

3. EXTRACTION OF SPECTRA FROM SZA AND LZA DATA

For gamma rays with energies of a few hundred GeV incident near the zenith, shower maximum occurs at about 7–9 km above sea level.[13] The Cerenkov light from such a shower forms a pool of light about 200 m in diameter at telescope altitude, 2.3 km for the Whipple Observatory. At large zenith angles, shower maximum occurs farther away from the telescope, which increases the area over which the Cerenkov light is distributed. The lower light density raises the telescope energy threshold, but for gamma rays with sufficient energy to produce enough light for triggering the collection area is substantially larger (Sommers & Elbert 1987). Since shower maximum occurs at a high altitude for LZA showers, the characteristic Cerenkov angles are smaller, resulting in a smaller Cerenkov light image nearer the center of the field of view of the camera. In this work we followed an established Whipple procedure in extracting spectra, specifically Method I as described in detail in Mohanty et al. (1998). The following parts are required: (1) a method for selecting gamma-ray–initiated shower images from a background of cosmic-ray–initiated shower images based upon image shape and orientation; (2) the effective telescope collection area for this selection method; (3) a method to estimate the initial gamma-ray energy for each event; and (4) the resolution function corresponding to this energy estimate. The method for selecting gamma-ray events should be relatively independent of the gamma-ray energy, E. The method of energy estimation should give good resolution and be relatively free of bias. These parts are described in the next two sections, and in the last subsection we show that spectra derived from Crab Nebula LZA observations agree with our standard SZA results published earlier.

3.1. *Energy Threshold, Selection Criteria, and Collection Area*

The Cerenkov imaging technique utilizes differences in focal plane image shapes to differentiate cosmic-ray background from gamma rays. The selection criteria (Mohanty et al. 1998) are based on image shape through the *width* and *length* parameters and on orientation through the *alpha* parameter. Compared with cosmic-ray images, gamma-ray images are generally narrower and shorter and point toward the center of the focal plane (see, e.g., Hillas 1985; Reynolds et al. 1993). The effective collection area of an imaging atmospheric Cerenkov telescope is limited not only by the dimension of the Cerenkov light pool on the ground but also by the image parameter cuts that are applied to increase the signal-to-noise ratio. The criteria are derived from the parameter distributions of simulated gamma-ray showers as a function of their total light intensity ("size" hereafter) in the photomultiplier camera. We set these criteria so that they keep 90% of gamma-ray images whose centroid is 0.°5–1.°1 (distance) from the center of the field of view for the 151 pixel camera. This distance restriction improves the correlation of energy with size. The cuts are scaled with size so that the efficiency for keeping gamma rays is approximately independent of energy.

The telescope is triggered when two of the inner 91 photomultiplier tubes give pulses within a triggering gate of 30 ns with 49 or more photoelectrons. The trigger electronics (Cawley et al. 1990) is difficult to model precisely. One of the problems is that the photomultiplier tube pulses include both Cerenkov light "signal" and Poisson-fluctuating night-sky noise "background," which causes the pulse shapes to vary. The pulses go both to a discriminator that fires when the pulse voltage crosses a preset threshold and to an integrating analog-to-digital converter that records the total charge, q, in the pulse (see Mohanty 1995). Because of the variation in pulse shape, there is no unique correspondence between pulse charge and peak voltage, effectively giving the discriminators a "fuzzy" edge having a width corresponding to 3.5 photoelectrons about a mean trigger point of 49 photoelectrons. In addition, if the discriminator levels are set very low, the background trigger rate for low-light events can be sensitive to night-sky brightness.

We avoid these difficulties using software padding (Cawley 1993) and by adding the additional software requirement that a signal corresponding to at least $D_{\rm soft} = 80$ photoelectrons is present in at least two pixels. This raises the telescope energy threshold, but the collection area can be readily calculated.

[13] Shower maximum is the region along the longitudinal development of the electromagnetic cascade with the maximum number of electrons and positrons.

The resulting SZA (20°) and LZA (55°–60°) telescope areas for events that pass both the triggering and image selection requirements are shown in Figure 1 for the 151 pixel camera. It is clear that only SZA measurements have sensitivity below 1 TeV, whereas the LZA measurements have better sensitivity beyond about 5 TeV. The LZA collection area shows a plateau between about 3 and 50 TeV. There is an SZA/LZA overlap region for cross calibration between about 1 and 10 TeV.

One concern is that we have properly extracted SZA spectra at all but the lowest energy point in Figure 1. The points at 260 and 380 GeV have significantly reduced collection area and hence might be unusually sensitive to small details in the simulations. We have looked for such sensitivities by varying (1) the telescope gain, (2) reflector optical resolution, and (3) background sky noise used in the simulations. The result is that neither the calculated collection area nor the extracted spectra change significantly if these parameters are varied over physically reasonable values. (Indeed, this is a basis for arriving at systematic errors.) Furthermore, the gamma-ray image parameter distributions extracted using on-off histograms (see Mohanty et al. 1998) agree with simulations. Thus the results appear to be robust.

3.2. *Energy Estimation and Resolution*

The accuracy of the energy reconstruction of gamma-ray primaries with a single imaging Cerenkov telescope is limited by the following effects: (1) fluctuations in the first interactions that cause the height of shower maximum to vary (hence the region where most of the Cerenkov light is emitted varies, causing fluctuations in the light density detected at ground), (2) the uncertainty in the shower core distance to the telescope, and (3) truncation of the shower images close to the edge of the field of view.

All three effects occur in a similar fashion for SZA and LZA observations; however, there are some differences: the central light emitting region for a LZA shower appears geometrically smaller in the camera because of its larger distance from the instrument and the smaller Cerenkov angles in the lower density atmosphere. Hence a bigger fraction of the Cerenkov light image is contained in the field of view.

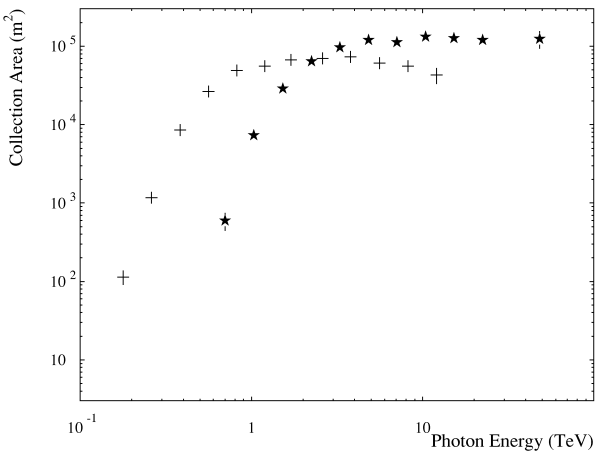

FIG. 1.—Collection areas for two different zenith angle ranges: 55°–60° (*stars*) and 20° (*crosses*) for the 151 pixel camera of the Whipple telescope in 1997. It should be noted that the 151 pixel camera has increased the collection area at 20° relative to the older 109 pixel camera because of its larger field of view.

Also, the smaller Cerenkov angles for LZA observations shift the center of gravity of images closer to the center of the field of view. Therefore, truncation effects are less important for LZA data.

Following Mohanty et al. (1998) we have found expressions for an energy estimate, $\tilde{E}$, as a function of ln (size) and distance, which are relatively free of bias and have good resolution. To a good approximation, for fixed energy E the distribution $\tilde{E}$ is lognormal (see Mohanty et al. 1998) with a width independent of E. It follows that the telescope resolution ΔE in standard deviations is given by $\Delta E/E = \sigma$, where σ is about 0.34 for SZA, and slightly better, about 0.29, for LZA.

3.3. *Atmospheric Effects*

Since Cerenkov light from showers at LZA passes through substantially more atmosphere than at SZA, the uncertainties in the atmospheric model may have correspondingly larger effects. There are four important extinction mechanisms:

1. The largest effect is Rayleigh scattering, for which the cross sections are well known. Variations arise because of changes in barometric pressure (typically a few percent) changing the column density along the line of sight from the telescope to shower maximum.
2. Ozone exists mainly at altitudes well above shower maximum, but the cross sections for UV absorption are very large and small concentrations extend into lower regions, which causes some absorption. Seasonal variations are of order 20%–25% at the Whipple Observatory latitude, and there are daily variations as well.
3. Absorption by O_2 becomes important below about 250 nm and removes almost all the light at shorter wavelengths. There are significant uncertainties in the absorption cross sections, but these uncertainties do not have a large effect because the absorption turns on rapidly, and in any case essentially all the light below 250 nm is absorbed.
4. Aerosols exist mainly at low altitudes with a scale height of roughly 1 km, and hence the observatory altitude of 2.3 km diminishes their effects. One of their primary characteristics is variability. If aerosol absorption were significant, one would expect significant variability in the telescope cosmic-ray–induced trigger rate, whereas this is usually stable to a few percent.

In order to estimate the effects of atmospheric uncertainties, we made some simple calculations using the atmospheric model used for the ARTEMIS project (Urban et al. 1996) and a simple aerosol parameterization used for the Fly's Eye experiment (Baltrusaitis et al. 1985). Assuming a Cerenkov light spectrum with wavelength-dependent mirror reflectivity and photocathode quantum efficiency folded in, the transmission for light from shower maximum (for 5 TeV gamma rays) to the telescope was calculated under various assumptions. The altitude of shower maximum for showers initiated by gamma rays at the zenith is 9 and 10 km for gamma-ray incidents at zenith angles of 60°. The results are given in Table 1. As can be seen from the table, atmospheric transmission from shower maximum at 60° is 78% of that at the zenith; however, changes in transmission due to fairly large increases in various extinction mechanisms is on the order of a few percent. This is small compared with the overall uncertainties in telescope gain of about 15% (Mohanty et al. 1998).

TABLE 1

RELATIVE ATMOSPHERIC TRANSMISSION AT SZA AND LZA

				TRANSMISSION	
RAYLEIGH (1)	AEROSOL (2)	O_2 (3)	OZONE (4)	$z = 0°$ (5)	$z = 60°$ (6)
1.....	1	1	1	1.0	0.78
1.03	1	1	1	0.99	0.77
1.....	4	1	1	0.96	0.73
1.....	1	4	1	0.98	0.76
1.....	1	1	4	0.93	0.74

NOTE.—Row (1) corresponds to standard atmospheric conditions; row (2) has the Rayleigh scattering column density increased by 3% (due to barometric pressure changes); row (3) has the aerosol concentration increased by a factor of 4; row (4) has the O_2 cross sections increased by a factor of 4; and row (5) has the ozone concentration increased by a factor of 4.

3.4. *The Crab Nebula Spectrum from LZA Data*

As a check on extraction of spectra from LZA observations, we have analyzed existing data for the Crab Nebula (1995–1997 with the 109 and the 151 pixel camera). In the angular range of 55°–60°, this consists of 8 hr of on-source data with corresponding off-source runs. When analyzed as described above, the resulting spectrum is shown in Figure 2. Also shown in the figure is the standard spectrum as given in Hillas et al. (1999a), which was derived using SZA observations. It is apparent that the two agree over the common energy range of about 1.1–10 TeV. A power-law fit to LZA data yields $J(E) = 3.78 \times 10^{-7} E^{-2.59 \pm 0.15 \pm 0.15}$ photons m^{-2} s^{-1} TeV^{-1}. The first set of uncertainties are statistical and the second are systematic and were calculated as in Mohanty et al. (1998). Based on the crab analysis and on our simulations of the effect of variations in the atmospheric model, we are confident about the SZA and the LZA energy estimate.

4. MARKARIAN 421 SPECTRUM

We have reanalyzed the SZA flare data of 1996 May 7 by using a more careful treatment of the telescope threshold region. The new spectrum is consistent with our previously published result but now includes two lower energy points extending down to 260 GeV instead of 560 GeV. The SZA flare data of 1996 May 15 were analyzed in exactly the same way. As pointed out previously, the threshold region is difficult to model, and to avoid it in the previous analysis we imposed a secondary software trigger level by requiring that two of the triggering tubes have signals corresponding to at least 50 photoelectrons ($D_{\rm soft} = 49$) and that the size was at least 400 photoelectrons.

In the present analysis, we impose no direct limitation on the signal size but instead require that $D_{\rm soft} = 80$. This also avoids the troublesome region, but with less cost in energy threshold. We have studied the effect on varying $D_{\rm soft}$ and found that the flux values in the spectrum are stable above a value of about 70. As $D_{\rm soft}$ is increased above 100, the flux values do not change within statistical errors, but these errors become significantly larger. We have also investigated another trigger configuration in which at least three tubes were required to have $D_{\rm soft}$ greater than 80. This again led to the same flux values within errors.

Finally, we reanalyzed the 1994/1995 Crab database and found that it is well fit over the energy range 0.3–10 TeV with a simple power-law consistent with the previous result given by Hillas et al. (1999a).

The spectral flux values derived from the intense flare of Markarian 421 at SZA are shown as stars in Figure 3. The

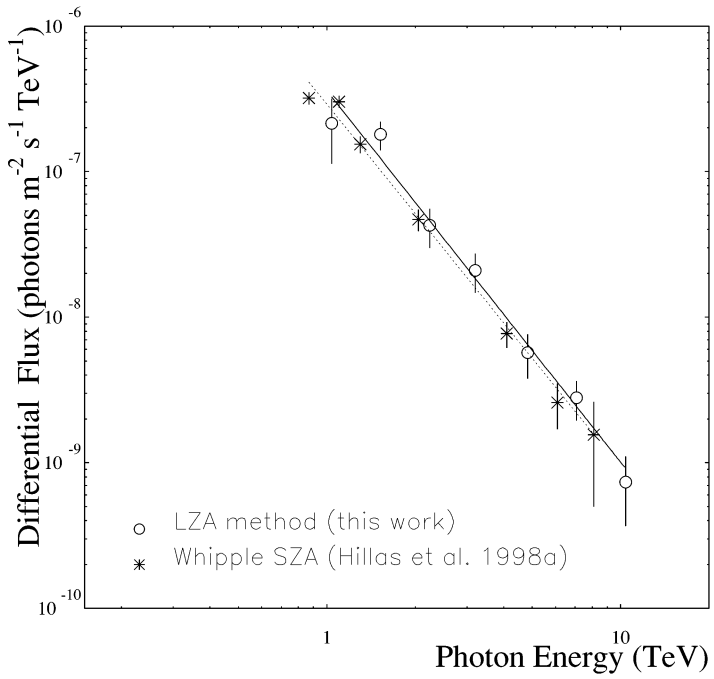

FIG. 2.—Energy spectrum of the Crab Nebula derived from LZA observations (*circles*) in comparison with the energy spectrum derived from SZA (*stars*) data (Hillas et al. 1999a). The spectral fits to the two data sets with a power law are consistent and are indicated by the solid and dashed lines.

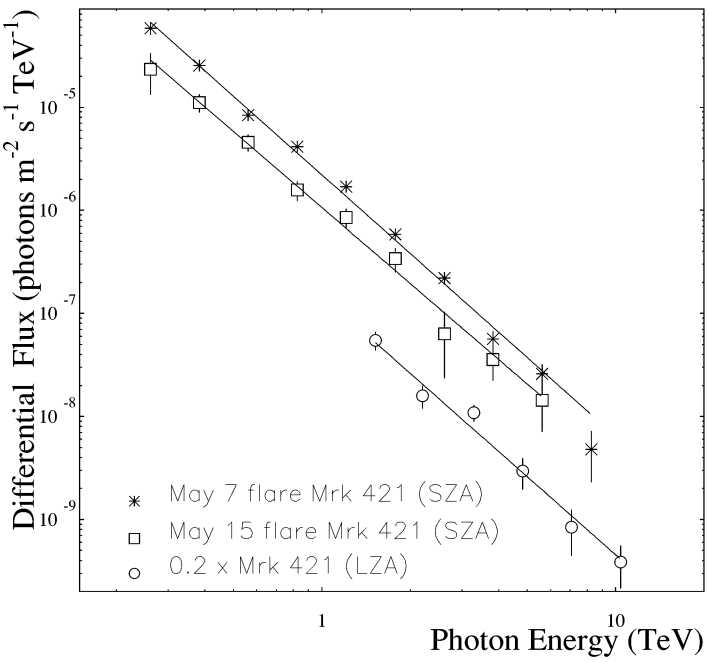

FIG. 3.—Energy spectra of Markarian 421 from the data of the big flare on 1996 May 7 (*stars*) and a short flare on 1996 May 15 (*squares*), and LZA data from flaring states in 1995 (*circles*). The flux of the LZA data has been presented as 0.2 of the absolute flux.

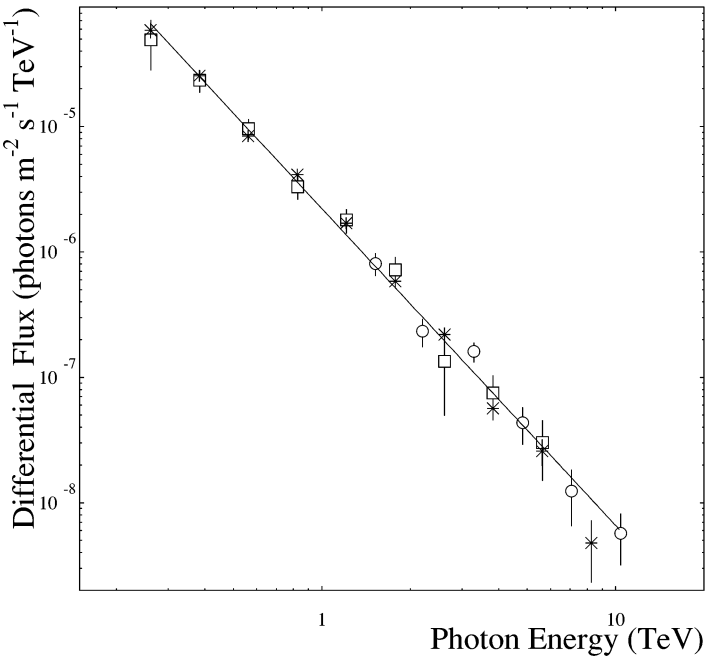

FIG. 4.—Energy spectrum of Markarian 421 combining the data from the big flare on 1996 May 7 (*stars*), the short flare on 1996 May 15 (*squares*), and a flaring state in 1995 (*circles*) at LZA. The absolute fluxes of the LZA data and the SZA data from 1996 May 15 have been normalized to the big flare data.

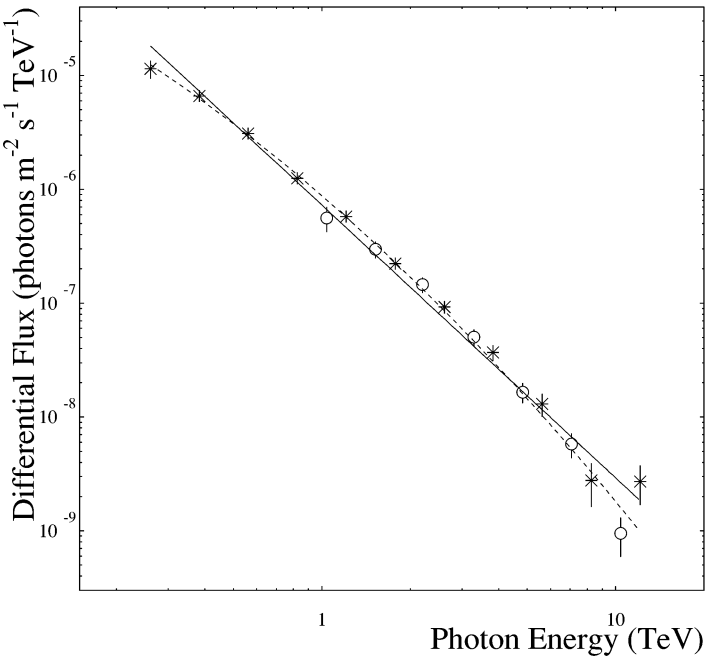

FIG. 6.—Energy spectrum of Markarian 501 using 15 hr of SZA data (*stars*) and 5 hr of LZA (*circles*) data. For this plot the absolute flux of the LZA data has been normalized to the SZA data. Both a simple power law (*solid line*) and a curved fit (*dashed line*) are shown in the figure.

data are fitted by $J(E) = 2.2 \times 10^{-6} E^{-2.54 \pm 0.04 \pm 0.1}$ photons m^{-2} s^{-1} TeV^{-1}, which gives a χ^2 of 22.8 for 8 d.o.f. (probability 0.005). This fit is marginal, perhaps indicating some curvature. The 1996 May 15 data are shown in the same figure as boxes and are fit by $J(E) = 1.0 \times 10^{-6} E^{-2.45 \pm 0.10 \pm 0.1}$ photons m^{-2} s^{-1} TeV^{-1}, which gives a χ^2 of 3.2 for 7 d.o.f. The LZA energy spectrum covers 1.5–10.4 TeV and is shown as open circles in the same figure. The LZA points can be fitted by a power law of the form $J(E) = 7.53 \times 10^{-7} E^{-2.52 \pm 0.18 \pm 0.15}$ photons m^{-2} s^{-1} TeV^{-1}, which gives a χ^2 of 4.9 for 4 d.o.f.

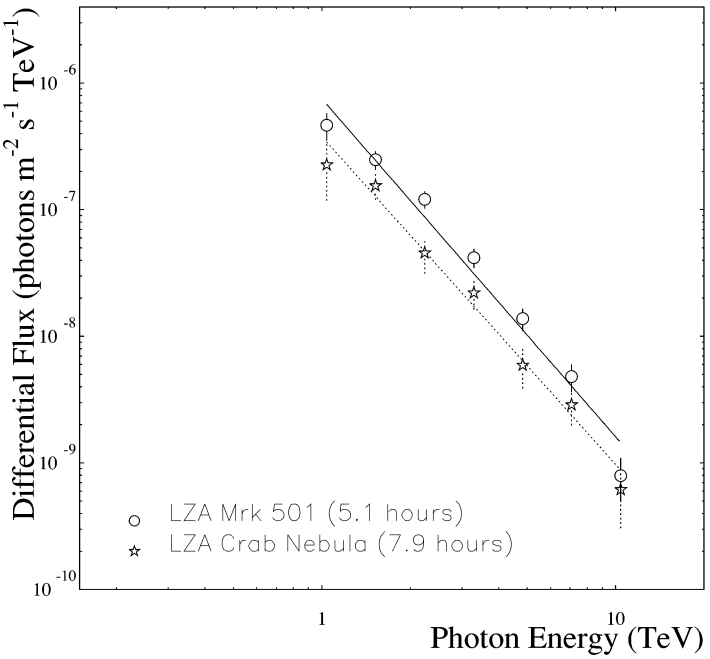

FIG. 5.—Energy spectrum of Markarian 501 (LZA data only) in comparison to the spectrum of the Crab Nebula derived with the same method. A power-law fit to the Markarian 501 data gives a $\chi^2 = 14.7$ for 5 d.o.f. (probability of 0.015).

Since all the spectral shapes are consistent we combine them in order to reduce the statistical uncertainties. In combining the two SZA data sets and the LZA data shown in Figure 4, the normalizations of the 1996 May 15 SZA data and the LZA were treated as free parameters, thus fixing the absolute normalization to the 1996 May 7 flare. The resulting fit is $J(E) \propto E^{-2.54 \pm 0.03 \pm 0.10}$ photons m^{-2} s^{-1} TeV^{-1}, which gives a χ^2 of 31.5 for 21 d.o.f. and a chance probability of 0.07. Thus the energy spectrum of Markarian 421 between 260 GeV and 10 TeV during flaring activity is consistent with a single power law. A curved fit for Markarian 421 yields

$$J(E) = (2.4 \pm 0.1 \pm 0.3) \times 10^{-6} \left(\frac{E}{1\ \mathrm{TeV}} \right)^{-2.47 \pm 0.04 \pm 0.05 - (0.28 \pm 0.09) \log_{10}(E)}$$

photons m^{-2} s^{-1} TeV^{-1}, with a χ^2 value of 21.5 for 20 d.o.f., which gives a chance probability of 0.4.

5. MARKARIAN 501 SPECTRUM

The Markarian 501 spectrum was analyzed in a similar way. The results for the 5.1 hr of LZA observations are shown together with the LZA spectrum for the Crab

Nebula in Figure 5. The flux level of Markarian 501 was on average ≈ 2 crab units during these observations, and the spectral slope is similar to that for the Crab spectrum. The spectrum extends up to 10 TeV and can be fitted between 1.1 and 10.4 TeV with a power law yielding $\chi^2 = 14.7$ for 5 d.o.f. (chance probability of 0.015): $J(E) = 7.53 \times 10^{-7} E^{-2.67 \pm 0.09 \pm 0.15}$ photons m^{-2} s^{-1} TeV^{-1}. The errors on the spectral index are given by a statistical uncertainty of ± 0.09, and a systematic uncertainty of ± 0.15. The slightly high value of χ^2 hints at curvature in the spectrum.

The LZA data (5.1 hr) can be combined with the SZA data (15 hr), treating the normalization of the former as a free parameter as described in the last section. This yields the spectrum given previously in Samuelson et al. (1998), which is shown in Figure 6. Fitting this data with a simple power law, $J(E) = 6.9 \times 10^{-7} E^{-2.41 \pm 0.025}$ photons m^{-2} s^{-1} TeV^{-1}, which gives $\chi^2 = 59.7$ for 15 d.o.f. with a chance probability of 2.5×10^{-7}. Including a curvature term yields $J(E) = (8.6 \pm 0.3 \pm 0.7) \times 10^{-7} E^{-2.22 \pm 0.04 \pm 0.05 - (0.47 \pm 0.07) \log_{10}(E)}$ photons m^{-2} s^{-1} TeV^{-1}, which gives $\chi^2 = 18$ for 14 d.o.f. with a chance probability of 0.2. As shown in Figure 6, the Markarian 501 spectrum is clearly curved. Spectral variability is not likely to account for the curvature; the superposition of two different power laws would result in a concave spectrum rather than a convex shape.

6. DISCUSSION: MARKARIAN 421 VERSUS MARKARIAN 501

The spectra derived from LZA and SZA data for Markarian 421 and Markarian 501 are shown in Figure 7. It is apparent from the figure that they differ; a χ^2 test places the chance probability that they arise from the same parent distribution at 4×10^{-3}. We conclude that the energy spectra of Markarian 421 and Markarian 501 during flaring activity are different.

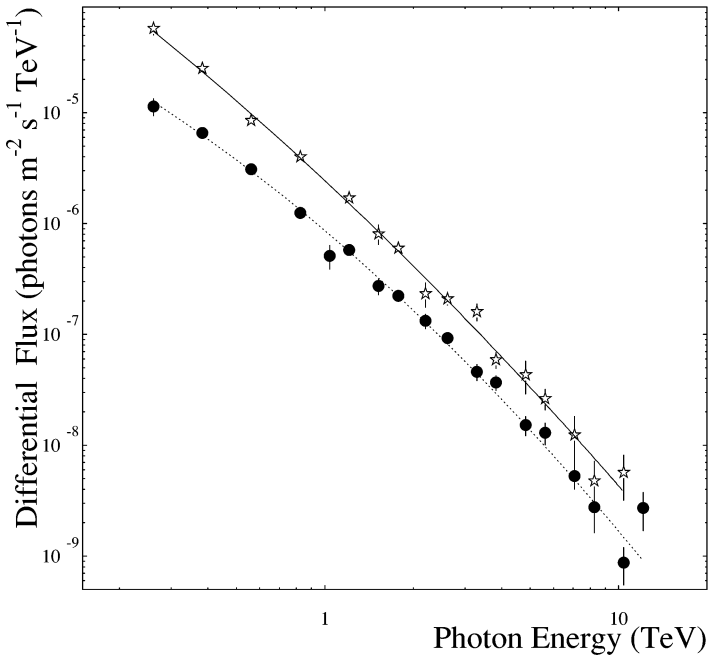

FIG. 7.—Energy spectrum of Markarian 501 (*circles*) and Markarian 421 (*stars*) are compared above. The solid line is a curved fit to the Markarian 421 fluxes, and the dotted line is a curved fit to the Markarian 501 fluxes.

Although Markarian 421 and Markarian 501 are at almost the same redshift, they do differ in their X-ray spectrum. Observations of Markarian 421 by the ASCA X-ray satellite experiment, although not contemporaneous with the data presented here, indicate an energy break in the synchrotron spectrum of 1.6–2.2 keV (Takahashi et al. 1996). In contrast, X-ray observations of Markarian 501 by *BeppoSAX* taken in 1997 April showed that its synchrotron power can peak at hard X-ray energies at 100 keV (Pian et al. 1997). These observations coincide with long-term flaring activity in TeV gamma rays (1997 February–1997 August) and indicated that synchrotron power from an AGN can peak at hard X-ray energies beyond 100 keV. In addition, Markarian 501 has been detected by the OSSE instrument aboard the *Compton Gamma Ray Observatory* at energies of 50–470 keV (Catanese et al. 1997), which clearly shows, for the first time, that synchrotron emission can peak above 100 keV.

At GeV energies, Markarian 421 is seen by EGRET (Lin et al. 1992), albeit weakly, whereas Markarian 501 is not seen (Catanese et al. 1997). Thus in terms of the synchrotron–inverse Compton models for which the GeV emission is from the inverse Compton mechanism, it would appear that both the synchrotron peak and the inverse Compton peak are shifted to higher energies, leaving the EGRET GeV energy sensitivity range in the gap between them for Markarian 501. As shown in Figure 7, in the energy range 260 GeV–10 TeV, the spectrum of Markarian 501 is harder at lower energies and shows more curvature than Markarian 421. In fact the latter is consistent with a straight line (i.e., pure power law). This is also consistent with the peak inverse Compton power occurring at higher energies for Markarian 501, nearer the range covering our measurements. We see no obvious contradiction of our results with a synchrotron–inverse Compton picture for the origin of the TeV radiation.

In order to probe intergalactic IR radiation via attenuation of TeV gamma rays, it is first necessary to know the intrinsic energy spectra of AGN. Spectral features such as the curvature of Markarian 501 cannot be ascribed a priori to this attenuation mechanism. This is clear because Markarian 421 and Markarian 501 have almost identical redshifts yet different spectra. The differences in their spectra can perhaps be explained in the context of the synchrotron–inverse Compton picture alluded to above (Hillas et al. 1999b). A proof of detection of the IR background radiation through a TeV photon absorption requires a detailed study of the spectrum of TeV blazars and their spectral variability; however, the IR limits (Biller et al. 1998) that allow for uncertainties in spectral shape are unchanged by this work.

In summary, we have shown that the TeV spectra of Markarian 421 and Markarian 501 differ significantly, the latter showing more curvature and a harder spectral slope below 2 TeV. Since the redshifts are almost identical, this difference can only be attributed to physics intrinsic to the objects themselves, and it is not inconsistent with a synchrotron-inverse Compton picture.

We acknowledge the technical assistance of K. Harris and E. Roache. This research is supported by grants from the US Department of Energy and by NASA, PPARC in the UK, and Forbairt in Ireland.

REFERENCES

Aharonian, F. A., et al. 1997, A&A, 327, L5
Baltrusaitis, R. M., et al. 1985, Nucl. Intrum. Methods Phys. Res., A240, 410
Biller, S. D., et al. 1998, Phys. Rev. Lett., 80, 2992
Bradbury, S. M., et al. 1997, A&A, A320, L5
Catanese, M., et al. 1997, ApJ, 487, L143
———. 1998, ApJ, 501, 616
Cawley, M. F. 1993, in Toward a Major Atmospheric Cerenkov Detector-II, ed. R. C. Lamb, 176
Cawley, M. F., et al. 1990, Exp. Astron., 1, 173
Gaidos, J. A., et al. 1996, Nature, 383, 319
Gould, R. J., & Schrèder, G. 1967, Phys. Rev., 155, 1408
Hillas, A. M. 1985, Proc. 19th Int. Cosmic-Ray Conf. (La Jolla, CA), 3, 445
Hillas, A. M., et al. 1999a, ApJ, in press
———. 1999b, in preparation
Krennrich, F., et al. 1995, in Toward a Major Atmospheric Cerenkov Detector, ed. M. Cresti, 161
———. 1997, ApJ, 482, 758
Lin, Y. C., et al. 1992, ApJ, 401, L61
Mannheim, K. 1993, Astron. Astrophys. Trans., 269, 67
Mohanty, G. 1995, Ph.D. thesis, Iowa State Univ.
Mohanty, G., et al. 1998, Astropart. Phys., 9, 15
Pian, E., et al. 1997, ApJ, 492, L17
Protheroe, R. J., Bhat, C. L., Fleury, P., Lorenz, E., Teshima, M., & Weekes, T. C. 1998, Proc. 25th Int. Cosmic-Ray Conf. (Durban), 8, 317
Punch, M., et al. 1992, Nature, 358, 477
Quinn, J., et al. 1996, ApJ, 456, L83
———. 1998, in preparation
Reynolds, P. T., et al. 1993, ApJ, 404, 206
Samuelson, F. W., et al. 1998, ApJ, 501, L17
Sikora, M., Begelman, M. C., & Rees, M. J. 1994, ApJ, 421, 153
Sommers, P., & Elbert, J. W. 1987, J. Phys. G., 13, 553
Stanev, T., & Franceschini, A. 1998, ApJ, 494, L159
Stecker, F. W., & De Jager, O. C. 1997, ApJ, 476, 712
Stecker, F. W., De Jager, O. C., & Salamon, M. H. 1992, ApJ, 390, L49
———. 1998, A&A, submitted
Takahashi, T., et al. 1996, Mem. Soc. Astron. Italiana, 67, 533
Thompson, D. J., et al. 1995, ApJS, 101, 259
Urban, M., et al. 1996, Nucl. Instrum. Methods Phys. Res., A368, 503
Zweerink, J., 1997, Ph.D. thesis, Iowa State Univ.
Zweerink, J., et al. 1997, ApJ, 490, L170